
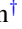


Anomalous neutralization characteristics in Na⁺ neutralization on Al(111) surfacesPinyang Liu, Liyuan Yin, Zheng Zhang, Bin Ding, Yuanqing Shi, Yin Li, Xin Zhang, Xiaoxun Song, Yanling Guo, Lin Chen ^{*} and Ximeng Chen [†]*School of Nuclear Science and Technology, Lanzhou University, Lanzhou 730000, China*Ivan K. Gainullin *Faculty of Physics, Moscow State University, Leninskie Gory 1 # 2, Moscow 119992, Russia*

Vladimir A. Esaulov

Institut des Sciences Moléculaires d'Orsay and CNRS, UMR 8214, Institut des Sciences Moléculaires d'Orsay, Orsay ISMO, Bâtiment 351, Université-Paris Saclay, 91405 Orsay, France

(Received 15 November 2019; revised manuscript received 26 February 2020; accepted 3 March 2020; published 26 March 2020)

The jellium model of free electron gas and its extended version have been widely used to understand the neutralization of alkali-metal ions on metal surfaces. We report an unexpected deviation from its prediction that we observed in the neutralization of Na⁺ ions scattering from an Al(111) surface. We find that the neutralization probability decreases monotonically with increasing ion velocity for the specular scattering condition, which is consistent with the well-known parallel velocity effect. However, the neutralization probability exhibits an unexpected bell shape with the variation of outgoing angle for a given incident energy. Calculations based on the jellium model using the rate equation and including the dynamic parallel velocity effect are presented. Their results agree with the velocity dependence of the neutral fraction, but completely fail in reproducing the angle dependence. This anomalous angle dependence could be due to the appearance of inelastic processes, corresponding to inner $2p$ electron promotion in hard encounters with Al atoms for large incidence angles, when the interatomic distances become small. This can lead to the formation of autoionizing Na states that result in the formation of extra Na⁺ ions, not accounted for in the jellium model.

DOI: [10.1103/PhysRevA.101.032706](https://doi.org/10.1103/PhysRevA.101.032706)**I. INTRODUCTION**

Charge transfer process is a basic interaction phenomenon between atomic projectiles and solid surfaces, and has attracted much attention [1–7]. The neutralization of scattered alkali-metal ions offers a novel method to investigate surface electronic properties of nanoclusters [8]. The ultrafast deexcitation and neutralization of highly charged ions from graphene was investigated [9]. Charge transfer of ion impact leads to low-energy electrons emission along the ion tracks [10,11], and their subsequent reactions with DNA play a crucial role in the DNA radiolysis [12]. Charge transfer is also involved in many aspects of technology applications, including low-energy ion scattering (LEIS) [13], secondary-ion mass spectroscopy (SIMS) [14], neutral beam heating of fusion plasma [15], high-current negative ion sources for spallation neutron source [16], and detection of low-energy neutrals in interplanetary and interstellar space [17].

The neutralization of alkali-metal ions on jelliumlike metal surfaces has been extensively studied both theoretically and experimentally [18–25]. The “standard” model of resonant charge transfer (RCT) has been widely used to describe the neutralization of alkali-metal ions on metal surfaces for the

nongrazing scattering geometry. In this approach the atomic level is considered to be broadened and shifted up due to the image potential as the ion-surface distance decreases. The resonant neutralization takes place when the atomic level of the alkali-metal ion is below the Fermi level of the surface for large ion-surface distances. Resonant ionization occurs when the atomic level shifts above the Fermi level at short distances. Therefore, the neutralization probability monotonically decreases with increasing incident energy due to shorter time available for electron capture. Previous theoretical works point out that energies and widths of atomic states for fixed atom-surface distances are strongly affected by the existence of band gaps and surface states of the metal surface [26–32]. It should be kept in mind that these effects are predicted for the case of fixed atom-surface distances. They may not always be observable in the case of scattering experiments because of nonadiabatic effects in scattering with finite velocities [26–29].

In recent years, the neutralization of Li⁺ and Na⁺ ions scattered from noble metal surfaces with high work functions has attracted much attention [20–24,33–37]. This followed the experimental observations of a very large neutralization probability and a nonmonotonic energy dependence that was not understandable in the standard jellium model. Several theoretical efforts have been devoted to explaining this open question [35–37]. In recent work on Li⁺/Cu(001), Li⁺/Cu(100),

^{*}chenlin@lzu.edu.cn[†]chenxm@lzu.edu.cn

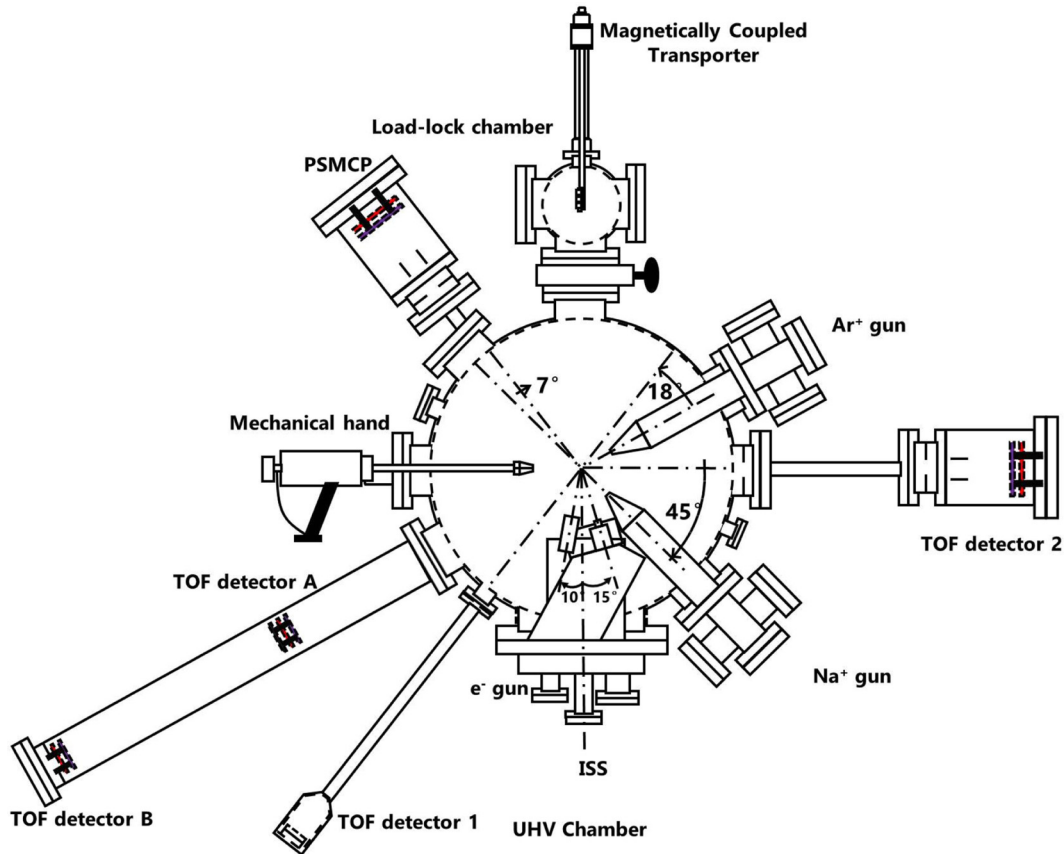


FIG. 1. Schematic diagram of the experimental setup.

and $\text{Li}^+/\text{Cu}(111)$ collision partners, a downward shift of the Li ionization level below the Fermi level caused by the short-range chemical interactions was proposed, and high neutral fractions at large exit energies can be explained in terms of this pronounced downshift of the energy level [35–37]. Insofar as lower work function surfaces are concerned, the jellium model has been usually tested for grazing specular scattering conditions, when the ion-surface distances remain large. However, more detailed tests involving nonspecular scattering conditions, probing different ranges of the atom-surface approach, have not been performed.

Thus the velocity dependence of Na^+ ion grazing scattering on $\text{Al}(111)$ surfaces has been studied in the past, and the calculation based on the jellium model correctly reproduced the experimental data [38–41]. However, the angle dependence has not been the subject of similar attention as compared to the velocity dependence. In this work, we studied low-energy Na^+ ion scattering in grazing scattering on a clean $\text{Al}(111)$ surface in specular and nonspecular scattering conditions. The neutralization probability was measured as a function of parallel velocity and outgoing angle to the surface. The experimental results are discussed in a theoretical framework using a wave-packet propagation approach, including the so-called “parallel velocity” effect [42] for grazing scattering, which takes into account modifications of the metal electron Fermi distribution as seen from the reference frame of the moving atom. This approach yields good agreement with the measured neutralization probability for grazing specular scattering conditions. However, experiments also reveal an

unusual and unexpected behavior of this probability as a function of exit angle, which could not be accounted for. We discuss this in more detail in the text.

For convenience, the atomic system of units is used by default, where $m_e = e = \hbar = 1$; e.g., 1 a.u. (atomic unit) of distance is equal to 0.53 \AA . The energies are given in electron volts, relative to the vacuum level ($E_v = 0$).

II. EXPERIMENT

The experiments were performed in an ion-scattering apparatus shown schematically in Fig. 1. A detailed description of the setup can be found elsewhere [21,43–46]. Briefly, the Na^+ ion beam with energy range from 0.2 to 5 keV was produced in a homemade Na^+ ion gun, and then collimated by several slits to the beam size of $1 \times 3 \text{ mm}^2$. Then the incident Na^+ ions collide with the $\text{Al}(111)$ sample which was mounted on a precision manipulator in an ultrahigh-vacuum (UHV) chamber with a pressure of about $3 \times 10^{-8} \text{ Pa}$. The scattered particles passed through the slits, and their charge states were analyzed by a parallel-plate electrostatic deflector. The charge-state-separated particles were then recorded by a one-dimensional position sensitive microchannel plate (PSMCP) detector. A multiparameter acquisition system (MPA-3) (FAST ComTec) was used for data collection. The detection efficiency of the PSMCP detector is assumed to be identical for particles with different charge states at the same impact energy [47–49].

The recorded position spectrum of scattered sodium particles is shown in Fig. 2. The neutralization probability or

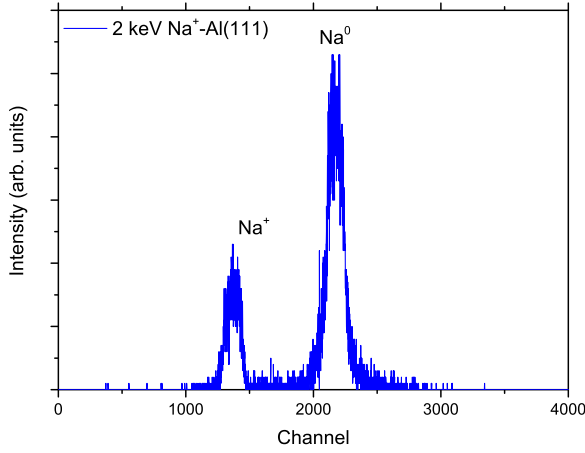


FIG. 2. The position distribution of scattered particles for 2-keV Na^+ ions in specular scattering on an Al(111) surface at a scattering angle of 7° . The spectrum does not show any negative ions.

neutral fraction is defined as $\Phi^0 = N(\text{Na}^0)/N(\text{Na}^0 + \text{Na}^+)$, where $N(\text{Na}^0 + \text{Na}^+)$ is the total number of scattered particles. No Na negative ions were observed. The crystal azimuth could not be rotated and experiments were performed for a random crystal orientation. The scattering angle is fixed at 7° and the incident (or exit) angle is varied.

In situ preparation of the Al(111) surface was accomplished by many cycles of 3-keV Ar^+ grazing sputtering and subsequent annealing at about 700 K (20 min) using electron bombardment. The typical beam spot size of Ar^+ ions is of $1 \times 3 \text{ mm}^2$ and the sample was moved by a stepping motor to achieve sputtering of the entire surface. The surface cleanliness was ascertained by time-of-flight scattering and recoiling spectroscopy (TOF-SARS) using 3-keV Ar^+ ions scattering on the sample with a scattering angle of 18° and an incident angle of 9° [50–54]. Once the recoil intensities of adsorbates such as H, C, O, Na, and S completely disappear, the surface is regarded as very clean (typically a sensitivity of 1% of the monolayer [50]). Figure 3 shows a typical TOF spectrum of clean Al(111) recorded by the TOF detector. The recoil peaks of impurity of H, C, O, Na, and S particles were located on the right-hand side of the big peak of scattered argon (see the inset). Furthermore, cross-checks of the surface cleanliness are made at the beginning, in the middle, and at the end of a series of measurements. Each cycle of the measurement starts from a freshly prepared clean Al(111). In this way we also ascertain that there is no Na implantation that could affect the surface work function.

III. DESCRIPTION OF THE THEORETICAL APPROACH

In Sec. III we describe the approach for the RCT calculation during grazing scattering. This description simplifies the discussion of the theoretical results in Sec. IV.

For the RCT calculation during grazing scattering the adiabatic approximation is used frequently [42]. Its core is that the RCT rate depends only on the ion-surface distance, but not on the ion velocity and the phase of the wave function. This assumption is reasonable for grazing scattering, because

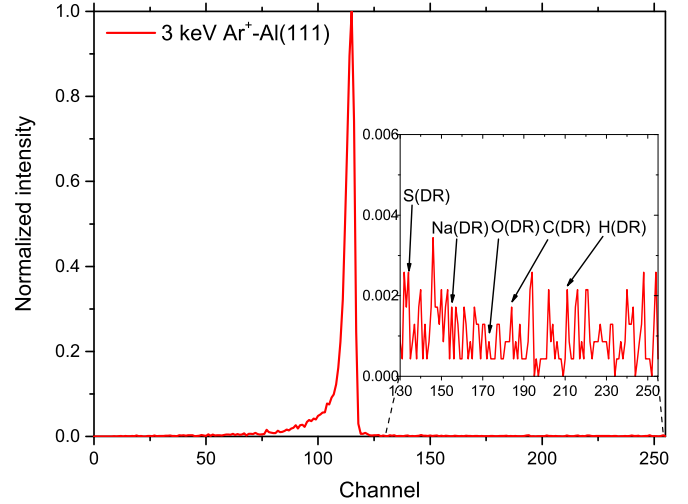


FIG. 3. TOF spectra for 3-keV Ar^+ ions scattering on Al(111) at an incident angle of 9° and a scattering angle of 18° . The big peak denotes the scattered Ar particles. The recoil intensities of adsorbates are shown in the inset. The intensity of these impurities falls in the background level.

the normal velocity of the ions is small (~ 0.01 a.u.) and nonadiabatic effects are not revealed.

For the grazing scattering geometry, the RCT is calculated by means of a rate equation [42]. To find the population of the atomic state we integrate the rate equation along the trajectory of ion motion [18]:

$$dP/dt = -\Gamma_{\text{loss}}(z)P + \Gamma_{\text{capture}}(z)(1 - P), \quad (1)$$

where z is the normal distance to the surface; $\Gamma_{\text{loss}}(z) = g_{\text{loss}}\Gamma(z)F_{\text{loss}}(z)$; $\Gamma_{\text{capture}}(z) = g_{\text{capture}}\Gamma(z)F_{\text{capture}}(z)$; $\Gamma(z)$ is the RCT ion level width; $F_{\text{loss}}(z)$ and $F_{\text{capture}}(z)$ are the electron loss and capture weights, respectively. The statistical factors are usually taken as $g_{\text{loss}} = 1$ and $g_{\text{capture}} = 2$ to account for the electron spin.

The procedure of calculation of $\Gamma(z)$ as a function of the ion-surface distance is described elsewhere [55,56]. In brief, we perform a series of auxiliary calculations of $\text{Na}^0 3s$ state decay in front of the metallic surface for a fixed ion-surface distance. The alkali-metal atom is considered as the hydrogen-like atom, consisting of a single *active electron* and a screened atomic core. We use a three-dimensional implementation of the wave-packet propagation method [57,58], which considers a direct study of the evolution of the active electron wave packet in the compound potential created by the surface and the projectile. Thus, we numerically solve the time-dependent Schrödinger equation (TDSE) with known initial conditions:

$$i \frac{d\psi(\mathbf{r}, t)}{dt} = \left[-\frac{\Delta}{2} + U(\mathbf{r}, t) \right] \psi(\mathbf{r}, t), \quad \psi(\mathbf{r}, 0) = \psi_0(\mathbf{r}), \quad (2)$$

where $U(\mathbf{r}, t) = V_{e\text{-ion}}(\mathbf{r}, t) + V_{e\text{-surf}}(\mathbf{r}) + \Delta V_{e\text{-surf}}(\mathbf{r}, t)$ is the time-dependent potential felt by the active electron. The TDSE numerical solution provides the time evolution of the system's wave packet $\psi(\mathbf{r}, t)$.

To calculate the electron loss and capture weights $F_{\text{loss}}(z)$ and $F_{\text{capture}}(z)$, we analyze the distribution of the active electron in the wave vectors space (k space). The active electron

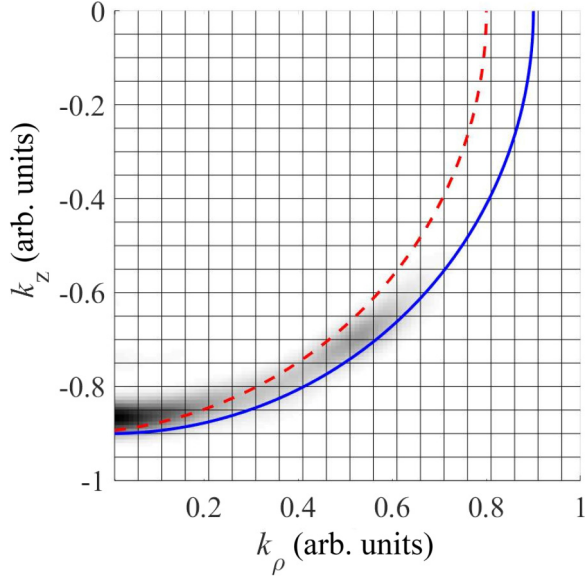


FIG. 4. Illustration of the electron loss and capture weights calculation. The shaded area shows the electron distribution $f(\mathbf{k})$ in k space for the $3s$ electron of Na, located at 10 a.u. from the Al(111) surface. The blue solid line corresponds to the Fermi sphere for Al(111) in the static case; the red dashed line to the Fermi sphere for $v_{\parallel} = 0.1$ a. u.

distribution inside the metal in k space is obtained by means of the Fourier transform of the electron's wave function:

$$f(\mathbf{k}, t) = \frac{1}{(2\pi)^{3/2}} \int_{z < 0} d\mathbf{r}^3 \cdot \psi(\mathbf{r}, t) \exp(-i\mathbf{k} \cdot \mathbf{r}). \quad (3)$$

It is important to note that the electron distribution in k space is quasistationary after the time ~ 100 a.u. from the interaction beginning. The example of the active electron distribution in k space is presented in Fig. 4. One can see that the electron distribution $f(\mathbf{k})$ is localized around the sphere of a certain radius k_a , which depends on the ion-surface distance (see the shaded area in Fig. 4). The expression $k_a^2/2$ gives the electron energy E_a , measured from the bottom of the conduction band. E_a increases with decreasing ion-surface distance for the upward-shifted Na ion level induced by the image potential [42]. The electron loss is possible when its distribution $f(\mathbf{k})$ is located outside the Fermi sphere of the metal—this means that the energy level of the active electron is located above the Fermi level; hence only resonant electron loss is possible, because there are no occupied electronic states inside the metal above the Fermi level. And vice versa, if the distribution of active electrons $f(\mathbf{k})$ is located inside the Fermi sphere, electron capture is possible.

Therefore, the weights of electron loss and capture are proportional to the part of the electron density located outside and inside the Fermi sphere, respectively [18]:

$$F_{\text{loss}} = \int_{|\mathbf{k}| > k_f} d\mathbf{k}^3 \cdot |f(\mathbf{k})|^2, \quad F_{\text{capture}} = \int_{|\mathbf{k}| < k_f} d\mathbf{k}^3 \cdot |f(\mathbf{k})|^2. \quad (4)$$

where $F_{\text{loss}} + F_{\text{capture}} = 1$.

Finally, to find the population of the Na $3s$ state, we integrate the rate equation (1) along the outgoing ion trajectory

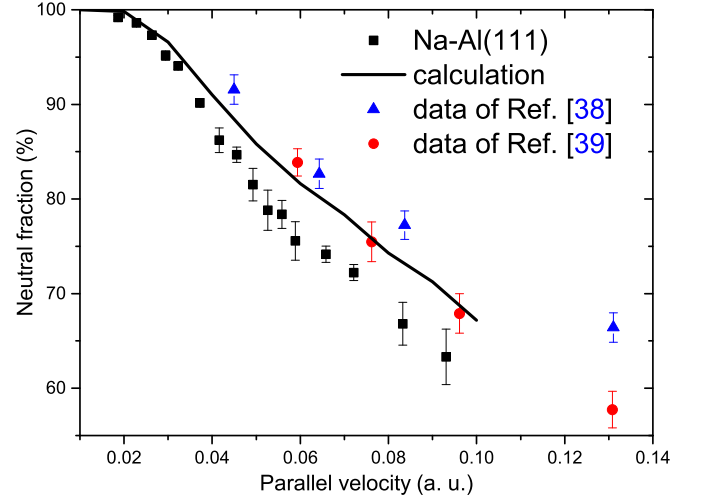


FIG. 5. Na^0 fraction from Al(111) surface as a function of parallel velocity for the specular scattering case ($3.5^\circ/3.5^\circ$). The solid line is the calculated result. The data in Refs. [38,39] are also presented for comparison.

for distances $z_{\min} = 3$ a.u. $< z < z_{\max} = 20$ a.u. Such an approximation is reasonable, because the final charge state of the atomic particle during grazing scattering forms at distances about 6–9 a.u. from the surface [28,42,59]. The auxiliary calculations show that the final Na^+ neutralization probability does not change when varying z_{\min} from 1 to 5 a.u., while the charge state near the surface ($z < 5$ a.u.) is “erased.” This feature is known as the “memory loss” effect [42], which is supported by several experimental studies [29,38,60,61], where the final fraction of scattered H^- and Li^+ ions does not depend on the primary ion beam charge state (negative or positive ions). The memory loss effect is a common feature of the RCT, which is related to extremely high RCT rate near the surface ($z < 5$ a.u.). According to our best knowledge, the memory loss effect is not limited to the specific projectiles. Moreover, the neutralization of the Na $3s$ state is similar to the neutralization of the Li $2s$ state, so the memory loss effect is expected for Na too. In fact, for the present system of Na^+ scattering on Al(111) surface, the memory loss effect also has no influence on the calculated results that well reproduce the experimental data [38–41]. The calculations stop when the ion moves away to 20 a.u. from the surface, where the RCT rate becomes negligible.

IV. RESULTS AND DISCUSSION

We measured the neutral fraction as a function of parallel velocity and exit angle for the Na^+ ions scattering on the Al(111) surface.

In Fig. 5 we show the neutral fraction as a function of parallel velocity in specular scattering ($3.5^\circ/3.5^\circ$; the perpendicular velocity $v_{\perp} \approx 1.1 - 5.7 \times 10^{-3}$ a.u.) with incident energies ranging from 0.2 to 5 keV. The measured neutral fraction decreases monotonously with increasing parallel velocity. Experimental results in Refs. [38,39] in this velocity range are also presented for comparison. The monotonic decrease of the neutral Na^0 fraction is similar to that observed in

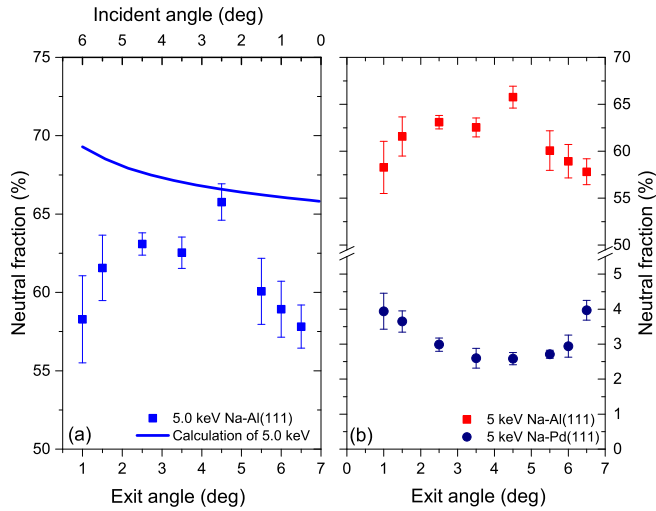


FIG. 6. (a) Na^0 fraction for 5.0-keV Na^+ scattered from the Al(111) surface as a function of exit (incident) angle for a fixed scattering angle of 7° . The solid line is the calculated result for 5.0-keV Na^+ ions. (b) The exit angle dependence of the neutral fraction for 5.0-keV Na^+ ions scattering on Al(111) and Pd(111) at the same scattering configuration.

the previous studies on Na^+ scattering from Al(111) for a fixed $v_\perp = 2.15 \times 10^{-3}$ a.u. [38], and for a grazing scattering geometry ($\approx 0.5^\circ/0.5^\circ$; $v_\perp \approx 0.16 - 0.81 \times 10^{-3}$ a.u. for the incident energy of 0.2–5 keV) [39]. The difference between the experimental data in Refs. [38,39] may be ascribed to the good preparation of the surface by the authors of Ref. [38], while the difference between our data and those in Ref. [38] could be explained by the effect of the perpendicular velocity component. With increasing perpendicular velocity, the neutral fraction decreases, as has been reported in Ref. [40].

Neutral fractions as a function of exit angle for the 5-keV energy are shown in Fig. 6(a). We observe an almost symmetrical bell-shaped dependence of the neutral fractions for 5-keV energy. The error bars are mainly due to statistics and are less than 5%. The decrease of neutralization fraction for 5-keV Na^+ ions from the plateau value of around 65% to about 57% is clearly larger than the statistical 5% error.

We have also measured the neutral fraction for Na^+ ions scattering on other metal surfaces like Pd(111) for the same scattering configuration (7°). The bell-shaped feature we observe for the Al case is very clearly different from the one observed for the Na–Pd(111) system as delineated by the comparative plot in Fig. 6(b). It is quite clear that as the exit angle increases, the neutral fraction from the Al(111) surface does not increase as for the other systems, but decreases.

This present inverse bell shape has not been observed previously for alkali-metal-ion neutralization. In our recent study on Na^+ neutralization [21], for Au(111), Pd(111), Cu(111), and Cu(110) surfaces, all the neutral fractions first decrease and then increase with the increase of incident angle for the studied 53° and 135° scattering angles. This was also observed in our previous study of Li ion neutralization on Au(110) and Pd(100) surfaces [20]. In particular, for Na^+ scattering on Cu(110) at a 53° scattering angle [21], although the work function of Cu(110), 4.49 eV, is smaller than the ionization

energy of Na (5.14 eV), the angle-dependent neutral fraction presents a similar trend to the Au(111), Pd(111) and Cu(111) surfaces, while for Al(111) with a smaller work function of 4.26 eV, fairly close to the Cu(110) surface, the angle dependence in this work differs from all mentioned above. In the previous study [21], the high neutralization at small incident angles (corresponding to a large exit angle), is due to the short interaction time for electron loss to the high work function surfaces like Au and Pd. At large incident angles, the high neutralization is enhanced by the parallel velocity effect [42].

Figure 5 shows the calculated Na^+ neutralization probability dependence on the parallel velocity component during Na^+ grazing scattering on Al(111). It is in good quantitative agreement with the experimental data. The decrease of the neutral fraction as a function of increasing velocity (energy) can be understood within the shifted Fermi spheres model (see Sec. III for details). The electron loss and capture weights depend on the electron distribution in k space. It is noted that, for the moving ion, the distribution of the active electron in k space is shifted by the value of the ion velocity (see Fig. 4) [62]. This is especially notable in the case of grazing scattering, when the parallel component of the ion velocity is relatively large, while the perpendicular velocity is one or two orders of magnitude smaller. In Fig. 4 one can see that for the static case the electron distribution $f(\mathbf{k})$ is located inside the Fermi sphere (solid blue line); it means that only electron capture is possible. While for the moving ion, due to the relative shift of the Fermi sphere (dashed red line) the electron loss and capture can occur concurrently. This is the key difference of RCT during the grazing scattering compared to the case of “near the normal scattering.” As a result, in the low ion velocity range the electron capture dominates and the neutralization probability is $\sim 100\%$, while for $v_\parallel \sim 0.1$ a.u. the neutralization probability reduces to 70% since concurrent electron capture and loss processes became possible.

It is noted that the difference between calculation results and the experimental data is about 10%. Such precision corresponds to the calculations presented in Ref. [39], while in Ref. [38] the calculation strictly matches the experimental data. There are two possible factors that can influence the calculations precision in our model. The first factor is the Fermi level position, which determines the Fermi sphere radius k_f ; in our calculations we used $E_f = -4.26$ eV. The second factor is the electron distribution $f(\mathbf{k})$ blurring, arising due to the finite size of the calculation grid. Note that in Ref. [38] the quasi-one-dimensional complex angular mode (CAM) method was used, where only one-dimensional angular electron distribution $f(\theta)$ is calculated and further three-dimensional distribution was implicitly calculated assuming the fixed radius of the active electron sphere k_a . Such an approach is suitable only for jellium surfaces, but it eliminates the electron distribution blurring.

As mentioned above there is an interesting unusual feature in our experiments, the bell-shaped dependence of Na^+ neutralization on the exit angle. This nonmonotonic angle dependence cannot be explained by the existing theory at present [21]. We present the calculated neutralization probability of 5-keV Na^+ ions scattered from the Al(111) surface in

Fig. 6(a), which decreases monotonously with the exit angle, in concordance with previous theoretical calculations [21,40]. The calculated result can be simply understood via two formulas as follows.

As mentioned above, in our case, the electron distribution reaches the quasistationary state. After the integration of Eq. (1), the final population of the atomic state $P(\infty)$ is approximated by the equilibrium occupation at the *freezing distance* R_s , which is

$$P_{\text{eq}}(R_s) = \frac{1}{\Gamma_{\text{loss}}(R_s)/\Gamma_{\text{capture}}(R_s) + 1}. \quad (5)$$

The freezing distance is

$$R_s = z_c \ln \left(\frac{\Gamma_0 z_c}{v_{\perp}} \right), \quad (6)$$

where z_c and Γ_0 are approximated parameters derived from ion level width $\Gamma(z) = \Gamma_0 \exp(-z/z_c)$. More details can be found in Ref. [42]. In brief, for $z < R_s$ the RCT rate is high and atom occupation $P(z)$ quickly reaches an equilibrium state, while for $z > R_s$ the RCT rate is low and atom occupation changes slowly. Therefore, the final neutralization fraction is determined by electron loss and capture weights at R_s .

In the nonspecular scattering condition, for a given velocity, the parallel velocity remains almost unchanged with the variation of exit angle from 1° to 7° . Such an almost-constant parallel velocity will reduce the Na^+ neutralization probability in the manner of concurrent electron capture and loss processes (shifted Fermi spheres model) mentioned above. The key point is that the perpendicular velocity of the projectile moving away from the surface will significantly increase. The increase of the perpendicular exit velocity with increasing exit angle leads to the reduction of the freezing distance R_s in Eq. (6). Considering that the Na ionization level shifts up with decreasing the ion-surface distance, the weight of electron loss slightly increases with the R_s . Therefore, following Eq. (5), a monotonic decrease of the neutralization fraction is obtained at larger exit angles.

To explain our observation, we need to seek other reasons for the decreasing behavior of neutral fraction with small exit angles. The effect of the image charge attraction on the neutral fraction during the grazing scattering should be taken into account, in particular for low-energy ions and relatively small exit angles. The induced angular shift between outgoing atoms and ions can be deduced from Ref. [63]. In Fig. 6(a) the bell shape of the angle dependence of the neutral fraction is obvious for 5-keV Na^+ ions, but the image charge effect can be neglected at this energy. In addition, for Na^+ ions scattering on a Pd(111) surface with the same scattering configuration (7°), the inversed bell-shaped angular dependence was found as shown in Fig. 6(b). The image charge effect should be the same for all the metallic systems studied and there should be nothing special about Al(111), so it cannot explain the bell shape of the angle dependence in the present work.

There is another factor that can influence the behavior of the angular dependence we observe, that until now has not been taken into account in our discussion. With increasing incidence angles the interatomic distance between the incoming Na ion and the target Al atoms decreases. Simulations using the KALYPSO code [64] using a Molière potential, for Na

incident on Al for angles between 3° and 7° and different crystal orientations, shows that the distance of closest approach decreases from around 1.6 to 0.7 a.u..

In our energy range and with increasing energy, this can lead to occurrence of inner-shell excitation processes involving promotion of the $2p$ electrons into excited higher-lying orbitals. This has been extensively studied for the isoelectronic to Na^+ , Ne^0 scattering on metals such as Mg, Al, etc., where the production of autoionizing $2p^4nl n'l'$ (Ne^{**}) states is observed [65,66] in our energy range. These are formed as a result of double $2p$ electron promotion for interatomic distances in typically the 1–1.5 a.u. range and followed by electron capture processes as the resulting ions recede from the surface. The autoionizing Ne^{**} doubly excited atom decays far from the surface leading to the production of extra Ne^+ . The same processes could lead to the production of excited autoionizing Na^{**} states that would lead to extra Na^+ observation. This has indeed been observed in Na^+ -Al collisions [67], and interpreted in the above terms using a calculated molecular orbital diagram. This would then lead to a decrease in the observed Na^0 production for large incidence angle impacts as observed.

Surface roughness plays an important role in inner-shell excitation processes; it is reported that the production of excited states in grazing scattering is favored for rougher surfaces [66]. Considering that the neutral fraction results are reproduced within the relative error below 5%, the effects of the *different* surface roughnesses should be minimized after the good preparation of the sample by the standard method as illustrated in Sec. II.

The electronic excitation is the possible reason for the bell-shaped dependence as shown in Fig. 6. Insofar as a quantitative evaluation is concerned this is complicated, as even if one could evaluate the yield of electrons corresponding to autoionizing states, these would not correspond to the total cross section of excitation (two and more electron excitations or ionizations) because of complicated multiple neutralization and Auger-type deexcitation processes [65,68]. This is beyond the scope of this study.

V. CONCLUSION

We have reported an experimental study for the neutralization in grazing scattering of 0.2–5-keV Na^+ ions on Al(111) surfaces at a scattering angle of 7° . Neutral fractions decrease monotonically with increasing velocity, while a bell shape presents with the variation of exit angles for a given incident energy. Calculations using the rate equations in the jellium model framework and including parallel velocity effects have been performed to understand the experimental data. The monotonic velocity dependence has been well reproduced using the jellium model, which, however, does not account for the falloff of the neutral fraction with decreasing outgoing angles. A possible explanation for this is that with the correspondingly increasing incidence angles, the Na-Al interatomic distances decrease below the threshold necessary for $2p$ electron promotion which then leads to the production of Na^{**} autoionizing states that decay far from the surface and contribute to increase the ion fraction.

ACKNOWLEDGMENTS

This work was supported by the National Natural Science Foundation of China (Grants No. 11474140 and No.

11405078). V.A.E. is grateful for the support of the Office of International Cooperation and Exchange, Lanzhou University (Grants No. GDT20186200141 and No. T2018006).

- [1] B. Obreshkov and U. Thumm, *Phys. Rev. A* **87**, 022903 (2013).
- [2] J. O. Lugo, E. C. Goldberg, E. A. Sánchez, and O. Grizzi, *Phys. Rev. B* **72**, 035432 (2005).
- [3] E. Sanchez, L. Guillemot, and V. A. Esaulov, *Phys. Rev. Lett.* **83**, 428 (1999).
- [4] S. Wethekam, H. Winter, D. Valdés, and R. C. Monreal, *Phys. Rev. B* **79**, 195408 (2009).
- [5] F. Bonetto, C. Gonzalez, and E. C. Goldberg, *Phys. Rev. B* **93**, 195439 (2016).
- [6] X. He and J. A. Yarmoff, *Phys. Rev. Lett.* **105**, 176806 (2010).
- [7] J. A. Gibbard, M. Dethlefsen, M. Kohlhoff, C. J. Rennick, E. So, M. Ford, and T. P. Softley, *Phys. Rev. Lett.* **115**, 093201 (2015).
- [8] G. F. Liu, Z. Sroubek, and J. A. Yarmoff, *Phys. Rev. Lett.* **92**, 216801 (2004).
- [9] R. A. Wilhelm, E. Gruber, J. Schwestka, R. Kozubek, T. I. Madeira, J. P. Marques, J. Kobus, A. V. Krasheninnikov, M. Schleberger, and F. Aumayr, *Phys. Rev. Lett.* **119**, 103401 (2017).
- [10] J. Schwestka, A. Niggas, S. Creutzburg, R. Kozubek, R. Heller, M. Schleberger, R. A. Wilhelm, and F. Aumayr, *J. Phys. Chem. Lett.* **10**, 4805 (2019).
- [11] J. F. Ziegler and J. P. Biersack, *The Stopping and Range of Ions in Matter* (Springer, Boston, MA, 1985).
- [12] B. Boudaïffa, P. Cloutier, D. Hunting, M. A. Huels, and L. Sanche, *Science* **287**, 1658 (2000).
- [13] H. H. Brongersma, M. Draxler, M. de Ridder, and P. Bauer, *Surf. Sci. Rep.* **62**, 63 (2007).
- [14] A. M. Belu, D. J. Graham, and D. G. Castner, *Biomaterials* **24**, 3635 (2003).
- [15] R. McAdams, *Rev. Sci. Instrum.* **85**, 02B319 (2014).
- [16] S. Henderson, W. Abraham, A. Aleksandrov, C. Allen, J. Alonso, D. Anderson, D. Arenius, T. Arthur, S. Assadi, J. Ayers, P. Bach, V. Badea, R. Battle, J. Beebe-Wang, B. Bergmann, J. Bernardin, T. Bhatia, J. Billen, T. Birke, E. Bjorklund *et al.*, *Nucl. Instrum. Methods Phys. Res., Sect. A* **763**, 610 (2014).
- [17] T. E. Moore, D. J. Chornay, M. R. Collier, F. A. Herrero, J. Johnson, M. A. Johnson, J. W. Keller, J. F. Laudadio, J. F. Lobell, K. W. Ogilvie, P. Rozmarynowski, S. A. Fuselier, A. G. Ghielmetti, E. Hertzberg, D. C. Hamilton, R. Lundgren, P. Wilson, P. Walpole, T. M. Stephen, B. L. Peko *et al.*, *Space Sci. Rev.* **91**, 155 (2000).
- [18] I. K. Gainullin, *Phys. Rev. A* **95**, 052705 (2017).
- [19] M. Pamperin, F. X. Bronold, and H. Fehske, *Phys. Rev. B* **91**, 035440 (2015).
- [20] L. Chen, J. Shen, J. Jia, T. Kandasamy, K. Bobrov, L. Guillemot, J. D. Fuhr, M. L. Martiarena, and V. A. Esaulov, *Phys. Rev. A* **84**, 052901 (2011).
- [21] L. Gao, Y. Zhu, Y. Shi, P. Liu, Y. Xiao, G. Li, Y. Liu, V. A. Esaulov, X. Chen, L. Chen, and Y. Guo, *Phys. Rev. A* **96**, 052705 (2017).
- [22] L. Chen, W.-B. Wu, P.-Y. Liu, Y.-Q. Xiao, G.-P. Li, Y.-R. Liu, H.-Y. Jiang, Y.-L. Guo, and X.-M. Chen, *Chin. Phys. B* **25**, 083401 (2016).
- [23] Y. Xiao, Y. Shi, P. Liu, Y. Zhu, L. Gao, Y. Guo, L. Chen, X. Chen, and V. A. Esaulov, *Nucl. Instrum. Methods Phys. Res., Sect. B* **450**, 73 (2019).
- [24] A. R. Canario, T. Kravchuk, and V. A. Esaulov, *New J. Phys.* **8**, 227 (2006).
- [25] J. A. Yarmoff, Y. Yang, and Z. Sroubek, *Phys. Rev. Lett.* **91**, 086104 (2003).
- [26] A. R. Canário, A. G. Borisov, J. P. Gauyacq, and V. A. Esaulov, *Phys. Rev. B* **71**, 121401(R) (2005).
- [27] A. G. Borisov, A. K. Kazansky, and J. P. Gauyacq, *Surf. Sci.* **430**, 165 (1999).
- [28] T. Hecht, H. Winter, A. G. Borisov, J. P. Gauyacq, and A. K. Kazansky, *Phys. Rev. Lett.* **84**, 2517 (2000).
- [29] L. Guillemot and V. A. Esaulov, *Phys. Rev. Lett.* **82**, 4552 (1999).
- [30] H. Chakraborty, T. Niederhausen, and U. Thumm, *Phys. Rev. A* **69**, 052901 (2004).
- [31] A. G. Borisov, J. P. Gauyacq, E. V. Chulkov, V. M. Silkin, and P. M. Echenique, *Phys. Rev. B* **65**, 235434 (2002).
- [32] K. Niedfeldt, E. A. Carter, and P. Nordlander, *Surf. Sci.* **600**, L291 (2006).
- [33] H. Hamoudi, C. Dablemont, and V. A. Esaulov, *Surf. Sci.* **602**, 2486 (2008).
- [34] T. Kravchuk, Yu. Bandourine, A. Hoffman, and V. A. Esaulov, *Surf. Sci.* **600**, L265 (2006).
- [35] F. J. Bonetto, E. A. Garcia, C. Gonzalez, and E. C. Goldberg, *J. Phys. Chem. C* **118**, 8359 (2014).
- [36] E. A. Garcia, M. A. Romero, C. Gonzalez, and E. C. Goldberg, *Surf. Sci.* **603**, 597 (2009).
- [37] C. Meyer, F. Bonetto, R. Vidal, E. A. Garcia, C. Gonzalez, J. Ferron, and E. C. Goldberg, *Phys. Rev. A* **86**, 032901 (2012).
- [38] A. G. Borisov, D. Teillet-Billy, J. P. Gauyacq, H. Winter, and G. Dierkes, *Phys. Rev. B* **54**, 17166 (1996).
- [39] R. Zimny, H. Nienhaus, and H. Winter, *Radiat. Eff. Defects Solids* **109**, 9 (1989).
- [40] A. G. Borisov, H. Winter, G. Dierkes, and R. Zimny, *Europhys. Lett.* **33**, 229 (1996).
- [41] H. Winter, *Z. Phys. D: At., Mol. Clusters* **17**, 109 (1990).
- [42] H. Winter, *Phys. Rep.* **367**, 387 (2002).
- [43] L. Chen, S. Qiu, F. Xiong, J. Lu, P. Liu, B. Ding, Y. Li, Y. Cui, Y. Guo, and X. Chen, *J. Chem. Phys.* **143**, 114703 (2015).
- [44] Q. Wang, S. Qiu, F. Xiong, Y. Li, B. Ding, Y. Guo, X. Chen, and L. Chen, *Eur. Phys. J. D* **69**, 210 (2015).
- [45] L. Chen, B. Ding, Y. Li, S. Qiu, F. Xiong, H. Zhou, Y. Guo, and X. Chen, *Phys. Rev. A* **88**, 044901 (2013).
- [46] L. Chen, P. Liu, Y. Xiao, L. Gao, Y. Liu, S. Qiu, F. Xiong, J. Lu, Y. Guo, and X. Chen, *Nucl. Instrum. Methods Phys. Res., Sect. B* **406**, 425 (2017).
- [47] R. S. Gao, P. S. Gibner, J. H. Newman, K. A. Smith, and R. F. Stebbings, *Rev. Sci. Instrum.* **55**, 1756 (1984).
- [48] H. C. Straub, M. A. Mangan, B. G. Lindsay, K. A. Smith, and R. F. Stebbings, *Rev. Sci. Instrum.* **70**, 4238 (1999).
- [49] N. Takahashi, Y. Adachi, M. Saito, and Y. Haruyama, *Nucl. Instrum. Methods Phys. Res., Sect. B* **315**, 51 (2013).

- [50] J. W. Rabalais, *Principles and Applications of Ion Scattering Spectrometry: Surface Chemical and Structural Analysis* (Wiley-Interscience, Hoboken, NJ, 2003).
- [51] L. Chen, J. Lu, P. Liu, L. Gao, Y. Liu, F. Xiong, S. Qiu, X. Qiu, Y. Guo, and X. Chen, *Langmuir* **32**, 12047 (2016).
- [52] L. Gao, Y. Zhu, Y. Shi, P. Liu, Y. Xiao, F. Ren, L. Chen, Y. Guo, and X. Chen, *Appl. Surf. Sci.* **428**, 1082 (2018).
- [53] L. Chen, S. Qiu, P. Liu, F. Xiong, J. Lu, Y. Liu, G. Li, Y. Liu, F. Ren, Y. Xiao, L. Gao, Q. Zhao, B. Ding, Y. Li, Y. Guo, and X. Chen, *Appl. Surf. Sci.* **387**, 1174 (2016).
- [54] F. Xiong, L. Gao, Y. Liu, J. Lu, P. Liu, S. Qiu, X. Qiu, Y. Guo, X. Chen, and L. Chen, *Vacuum* **137**, 23 (2017).
- [55] I. K. Gainullin, *Phys. Rev. A* **100**, 032712 (2019).
- [56] I. K. Gainullin and M. A. Sonkin, *Phys. Rev. A* **92**, 022710 (2015).
- [57] I. K. Gainullin and M. A. Sonkin, *Comput. Phys. Commun.* **188**, 68 (2015).
- [58] I. K. Gainullin, *Comput. Phys. Commun.* **210**, 72 (2017).
- [59] T. Hetch, H. Winter, A. G. Borisov, J. P. Gauyacq, and A. K. Kazansky, *Faraday Discuss.* **117**, 27 (2000).
- [60] M. Maazouz, A. G. Borisov, V. A. Esaulov, J. P. Gauyacq, L. Guillemot, S. Lacombe, and D. Teillet-Billy, *Phys. Rev. B* **55**, 13869 (1997).
- [61] A. G. Borisov, D. Teillet-Billy, and J. P. Gauyacq, *Phys. Rev. Lett.* **68**, 2842 (1992).
- [62] J. N. M. Van Wunnik, R. Brako, K. Makoshi, and D. M. Newns, *Surf. Sci.* **126**, 618 (1983).
- [63] H. Winter, *J. Phys. Condens. Matter* **8**, 10149 (1996).
- [64] M. A. Karolewski, *Nucl. Instrum. Methods Phys. Res., Sect. B* **203**, 211 (2003).
- [65] S. Lacombe, V. Esaulov, L. Guillemot, O. Grizzi, M. Maazouz, N. Mandarin, and V. N. Tuan, *J. Phys.: Condens. Matter* **7**, L261 (1995).
- [66] O. Grizzi, E. A. Sánchez, J. E. Gayone, L. Guillemot, V. A. Esaulov, and R. A. Baragiola, *Surf. Sci.* **469**, 71 (2000).
- [67] M. Minniti, M. Comisso, A. Sindona, E. Sicilia, A. Bonanno, P. Barone, R. A. Baragiola, and P. Riccardi, *Phys. Rev. B* **75**, 045424 (2007).
- [68] V. A. Esaulov, *J. Phys. Condens. Matter* **6**, L699 (1994).